

Observing a Phase Transition on a Coherent Ising Machine

Hiroki Takesue^{1,†,*}, Yasuhiro Yamada^{1,†,‡}, Kensuke Inaba¹, Takuya Ikuta¹, Yuya Yonezu¹, Takahiro Inagaki¹, Toshimori Honjo¹, Takushi Kazama², Koji Enbutsu², Takeshi Umeki², and Ryoichi Kasahara²

¹*NTT Basic Research Laboratories, NTT Corporation,*

3-1 Morinosato Wakamiya, Atsugi, Kanagawa 243-0198, Japan and

²*NTT Device Technology Laboratories, NTT Corporation,*

3-1 Morinosato Wakamiya, Atsugi, Kanagawa 243-0198, Japan[‡]

(Dated: January 31, 2023)

A coherent Ising machine (CIM) is known to deliver the low-energy states of the Ising model. Here, we investigate how well the CIM simulates the thermodynamic properties of a two-dimensional square-lattice Ising model. Assuming that the spin sets sampled by the CIM can be regarded as a canonical ensemble, we estimate the effective temperature of the spins represented by degenerate optical parametric oscillator pulses by using maximum likelihood estimation. With the obtained temperature, we confirmed that the thermodynamic quantities obtained with the CIM exhibited a phase-transition-like behavior that better matches the analytical and numerical results than the mean field one.

PACS numbers: 42.65.Yj, 42.50.Dv, 42.50.p, 05.90.+m

Recently, “Ising machines”, which simulate the Ising model by using physical systems that substitute for the Ising spins, have been drawing attention as a way to circumvent the apparent plateau in the progress of digital computers [1]. Among the various optical Ising machines demonstrated so far [2–11] is the coherent Ising machine (CIM) [2–6], in which a network of degenerate optical parametric oscillators (DOPO) is used to simulate the Ising model. It has been shown that the CIM delivers the low-energy states of the Ising model [3–6].

On the other hand, it is important to understand how well the CIM reproduces the characteristics of the Ising model. So far, we have simulated a two-dimensional (2D) square-lattice Ising model at low temperature on the CIM in order to understand the machine’s dynamics in its search for the low energy states [12]. We have also investigated the behavior of a 2D square lattice in an external magnetic field on the CIM and found that the results matched the analytical solutions and Monte-Carlo simulations [13]. The main motivation of this study is to clarify whether a CIM exhibits a thermal phase transition of the ferromagnetic 2D Ising model on a square lattice, which is one of the most prominent thermodynamic phenomena observed in the Ising model. The analytical solution for the 2D square lattice, as conceived by Onsager, exhibits a clear phase transition at $(\beta J)_c = \frac{\ln(1+\sqrt{2})}{2} \simeq 0.44$, where β and J denote inverse temperature and the spin-spin interaction coefficient, respectively [14]. This analytical solution is based on the assumption that the ensemble of Ising spins are canonically distributed in a thermal bath. Therefore, an investigation of phase transitions on a CIM may also lead to a better understanding of the energy distribution of the

“spins” represented by DOPOs.

Another motivation of this work is to see if the performance of the CIM can be simulated using the mean-field (MF) dynamics, as described in [1, 15]. It is known that the MF solution to the 2D square lattice Ising model exhibits a phase transition at $(\beta J)_{c, MF} = 1/4$, which is clearly different from the exact analytical and numerical solutions. Thus, we should be able to learn if there is a difference between the CIM and the “mean field solver” through this study.

In this Letter, we experimentally demonstrate that the CIM can simulate the phase transition of a 2D square-lattice Ising model. By varying the amplitude of the injected optical pulses for coupling the DOPOs, we could change the effective inverse temperature β that the DOPO pulses represent as the Ising spins. As a result, we observed a clear phase transition of the magnetization, which better matched the theoretical curves obtained with the exact analytical solution and numerical simulation based on the Wang-Landau (WL) method [16] than the mean field one.

Figure 1 (a) shows the experimental setup (for details of the setup, see [13]). The CIM consists of a fiber ring cavity that contains a phase sensitive amplifier (PSA) based on a periodically poled lithium niobate (PPLN) waveguide, two 9:1 fiber couplers, an 0.1-nm width optical bandpass filter, a piezo-based phase shifter for cavity locking, and a 1-km optical fiber. 780-nm, 1-GHz-repetition pump pulses with a ~ 20 -ps temporal width are launched into the PSA. When pumping starts, the PSA generates squeezed vacuum pulses through signal-idler degenerate parametric downconversion in the PPLN waveguide. The squeezed vacuum pulses circulates in the ring cavity while undergoing phase sensitive amplification. As a result, the pulse amplitude saturates after many circulations in the cavity to form 5055 DOPO pulses multiplexed in the time domain. Among the 5055 pulses, 512 (referred to as “signal pulses” hereafter) are

* hiroki.takesue@ntt.com

† yshr.yamada@ntt.com

‡ These authors contributed equally to this work.

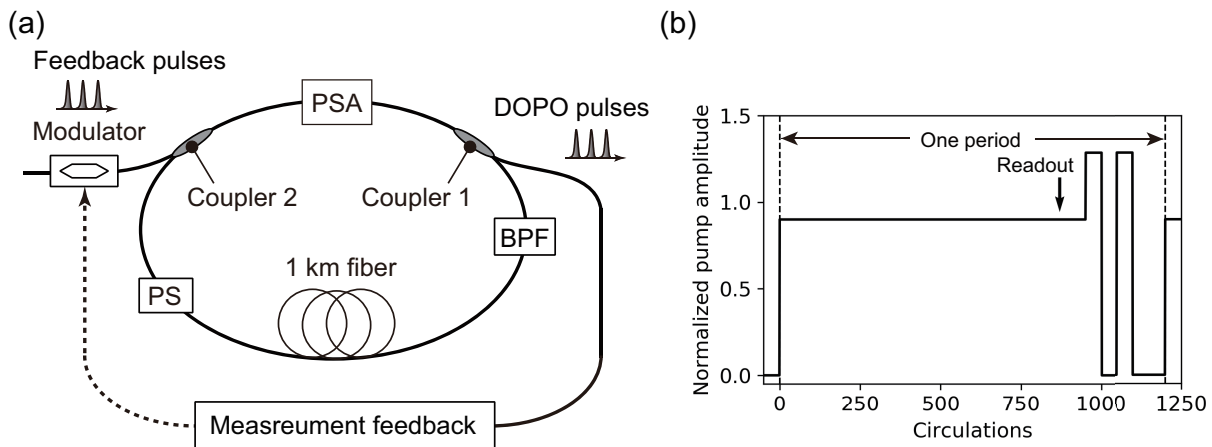


FIG. 1. Coherent Ising machine with measurement feedback. (a) Experimental setup. PSA: phase sensitive amplifier. BPF: optical bandpass filter with 0.1-nm bandwidth. PS: phase shifter. The measurement-feedback part includes a balanced homodyne detector, an analog-to-digital converter, an FPGA, and a digital-to-analog converter. (b) Temporal change in the normalized pump amplitude for generating the DOPO pulses used for computation as a function of the number of circulations in the fiber cavity. The vertical arrow indicates the readout point of the DOPO pulses (870th circulation).

periodically turned on and off to simulate the given Ising model many times, while the remaining pulses oscillate continuously. The phase of the DOPO pulses takes only either 0 or π phase relative to the pump phase as a result of the repetitive phase sensitive amplification. By assigning phase 0 (π) as spin up (down), the DOPO phase can represent an Ising spin state. The “spin-spin interaction” among the DOPO pulses are implemented with the measurement-feedback scheme [3, 4]. In this scheme, a portion of the DOPO pulse energy is split by Coupler 1 in the ring cavity and one of the quadrature amplitudes is measured for all DOPO pulses by using a balanced homodyne detector. The measurement results are then analog-to-digital converted and input into a fast matrix calculation circuit realized with a field programmable gate array (FPGA). Here, the spin-spin interaction matrix for a given Ising model of size N is uploaded to the FPGA in advance. The FPGA performs the multiplication of the $N \times N$ matrix and an N -element vector corresponding to the measurement results on the N DOPO pulses, so that a feedback signal for each DOPO pulse is obtained in the next round trip. The feedback signal is then used to modulate the amplitude and phase of an optical pulse whose wavelength is the same as that of the DOPO pulse in the cavity, and the optical pulse is launched into the corresponding DOPO pulse through Coupler 2. Here, we denote the amplitude of the injection pulse relative to the DOPO pulses in the cavity by J_{inj} . We repeat the measurement-feedback procedure for each circulation in the cavity. The DOPO pulses circulate 1000 times in the cavity in accordance with the temporal schedule of the pump amplitude shown in Fig. 1 (b). The final readout of the DOPO pulse amplitudes is undertaken at the 870th circulation. With the current measurement-feedback system, we can implement all possible combinations of two-body interactions among 512 signal pulses with an 8-bit

resolution.

We implemented an N -spin 2D square lattice with periodical boundary conditions on the CIM. The vertical and horizontal links had the same coupling strength. Montroll et al. showed that the spontaneous magnetization $M = \sum_i \sigma_i (\sigma_i = \{-1, 1\})$ of the 2D square-lattice Ising model has an exact solution at the thermodynamic limit, given by [17]

$$M = \left[1 - \frac{1}{\sinh^4 2\beta J} \right]^{1/8}. \quad (1)$$

This equation indicates that the model exhibits a phase transition at $(\beta J)_c \simeq 0.44$. In our experiment, the feedback pulse amplitude J_{inj} is supposed to be proportional to J . Therefore, we ran the CIM many times for various J_{inj} values. The value of J_{inj} is proportional to the amplitude of the FPGA output signal denoted by g , which can take an integer value in the range between 0 and 127. Consequently, we obtained samples of spin sets from which we then obtained the internal energy U (or the average of the Ising energies) and magnetization values for each J_{inj} . However, the increase in J_{inj} has a similar effect as increasing the pump amplitude for DOPO pulses. As a result, the effective inverse temperature β of a “spin” represented by a DOPO pulse changes, which means that a change in J_{inj} affects both β and J . Hereafter, we assume that $J = 1$ and the effect of a change in J_{inj} is reflected in β . Assuming that the sampled energies are from a canonical distribution, $P(E|\beta)$, the energy distribution at the effective inverse temperature β and $D(E)$, the density of states (DOS), can be related to β with the following equation:

$$P(E|\beta) = D(E) \frac{e^{-\beta E}}{Z}. \quad (2)$$

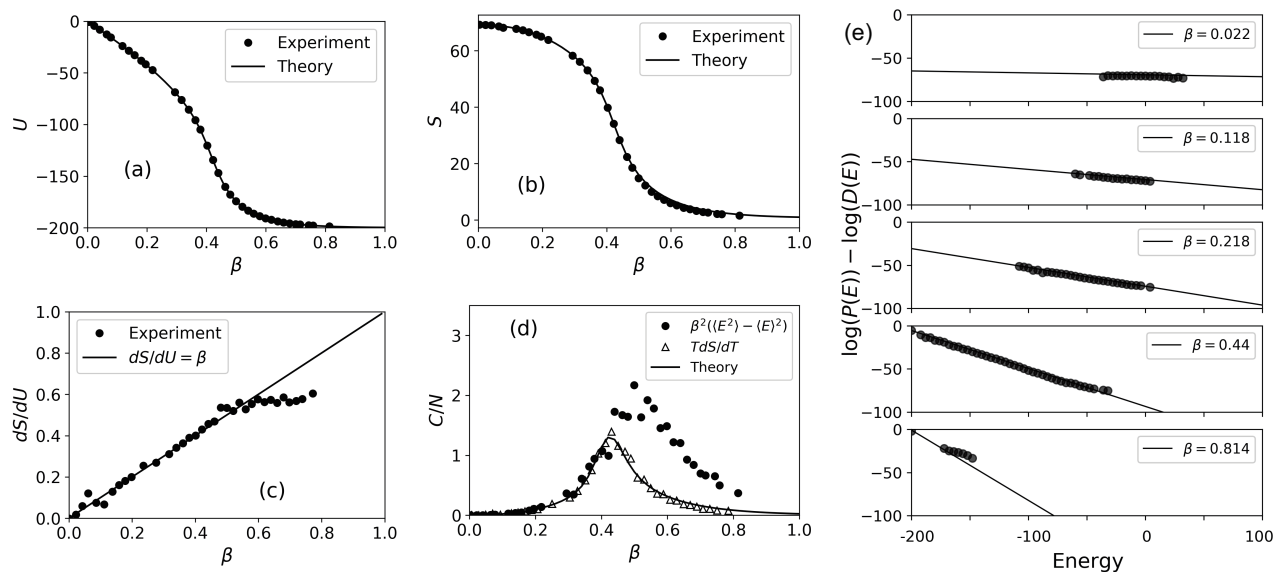


FIG. 2. Experimental results. (a) Internal energy U as a function of inverse temperature β . β is estimated by fitting the experimentally obtained U to the theoretical U curve. (b) Experimentally obtained entropy S as a function of the estimated β . (c) dS/dU as a function of the estimated β . (d) Specific heat as a function of β . (e) $\log P(E|\beta)/D(E)$ as a function of energy, where $P(E|\beta)$ denotes the energy distribution at an inverse temperature β . The lines correspond to theoretical values calculated using the estimated β and the DOS obtained with the WL method.

Here, $Z = \sum_E D(E)e^{-\beta E}$ is the partition function, and $D(E)$ of the given graph can be calculated using the WL method [16]. Under this assumption, we estimate the inverse temperature β using maximally likelihood estimation. The value of β estimated with this procedure gives an internal energy (or sample average of the Ising energy) that coincides with the theoretical value $U = \langle E \rangle = \sum_E EP(E|\beta)$. We plotted the magnetization, entropy $S = -\sum_E P(E) \ln \frac{P(E)}{D(E)}$, and specific heat C (defined later) as a function of β estimated for each sample set. Regarding the magnetization, we used the root mean square (RMS) of $M = \frac{1}{N} \sum_i \sigma_i$.

We implemented a 2D square-lattice Ising model with $N = 100$ (10×10). The periodical boundary conditions were implemented by taking advantage of the flexible spin-spin interaction enabled by the measurement feedback. We embedded four $N = 100$ graphs together with a 32-node bipartite graph that was used as “monitor graph”. These graphs were multiplied with a 432×432 random permutation and spin flip matrix so that the temporal positions and the signs of the spins were randomized to avoid the formation of ferromagnetic states due to experimental imperfections such as reflections of light inside the fiber cavity.

We operated the CIM so that it performed 256 computations in a single batch of measurements, which yielded 1048 spin sets for the 100-node 2D Ising model. In order to extract results obtained when the CIM stably operated, we eliminated the results when the obtained Ising energy of the monitor graph did not reach the ground state. We then used the energies of the remaining results

in the batch to estimate β . We set 22 values of the FPGA coupling coefficient g ranging from 0 to 125 and obtained ten batches of results for each g value. We repeated this procedure four times, which means that we accumulated 40,960 spin sets for each g value. On average, $\sim 8\%$ of the spin sets passed the filtering by the monitor graph.

Figure 2 (a) shows the internal energy as a function of the estimated β , which fits the theoretical curve as a natural result of the maximal likelihood estimation. The experimental entropy as a function of the estimated β is shown by circles in Fig. 2 (b). The experimental data exhibit a clear fit with the theoretical curve, suggesting that not only the average energy but also the energy distribution agree with the theory based on the canonical distribution assumption. Using the $\beta - U$ and $\beta - S$ relationships, we plotted an $S - U$ curve, from which we obtained the thermodynamic inverse temperature defined as dS/dU . The relationship between the obtained dS/dU and estimated β is shown in Fig. 2 (c), which indicates that the estimated temperatures were close to the thermodynamic temperature for β up to ~ 0.6 .

The experimental and theoretical specific heats are shown in Fig. 2 (d). The circles show the experimental specific heat derived using the Ising energies and the statistical-mechanical relationship $C_{\text{stat}} = \beta^2(\langle E^2 \rangle - \langle E \rangle^2)$, and the triangles denote another set of experimental values obtained from the estimated entropy (Fig. 2 (b)) and the thermodynamic relationship $C_{\text{thermo}} = TdS/dT$. The circles form a clear peak structure that is a characteristic of the theoretical specific heat as a function of temperature, but at a clearly larger β . Since C_{stat} is a quantity that is proportional to the variance of the

energy, experimental instability enhanced at around the transition point may have caused the discrepancy from the theory. On the other hand, C_{thermo} plotted as the triangles fits the theoretical curve very well, which suggests that the spin sets produced by the CIM satisfy the thermodynamic relationship.

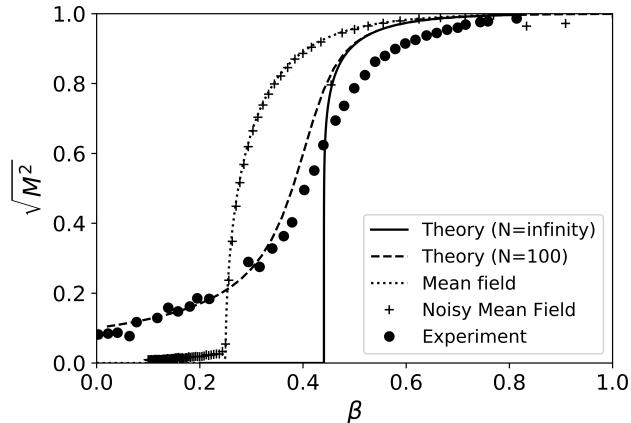


FIG. 3. Root mean square magnetization as a function of β . The dots plot the experimental spontaneous magnetization as a function of the estimated β . The solid and dashed lines are the theoretical curve for the thermodynamic limit based on Eq. (1) and the numerical calculations based on the WL method for $N = 100$. The dotted line and + symbols respectively correspond to the MF theory curve and the simulation with noisy MF annealing [15].

Using the estimated β , we plotted $\log P(E|\beta) - \log D(E)$ as a function of energy, which should be a linear function with slope β . The results are shown in Fig. 2 (e); the experimentally observed distributions fit the theoretical line for the canonical distribution at a β around the theoretical transition point (~ 0.44) or smaller. In contrast, at a relatively larger β ($\simeq 0.81$), we observed a clear discrepancy from the theoretical line. This suggests that the effective temperatures obtained in our experiment are close to the temperature obtained by statistical mechanics with the canonical distribution assumption, except at temperatures significantly below the transition temperature. Note that this tendency resembled the one observed in the $\beta - dS/dU$ curve shown in Fig. 2 (c), where the thermodynamic inverse temperatures are smaller than the effective β for $\beta > \sim 0.6$. We emphasize that it is nontrivial that the present diffusive system satisfies the canonical distribution assumption throughout most of the temperature region. The results show good agreement among the experimentally estimated temperature, thermodynamic temperature, and statistical-mechanics

temperature under the canonical distribution assumption, except at very low temperatures.

Next, we plotted the RMS magnetization $\sqrt{M^2}$ as a function of the effective β . As is apparent from Fig. 3, the experimental result exhibited a clear phase-transition-like behavior in the finite-sized system with the critical temperature at $\beta \sim 0.42$. It also confirmed that the RMS magnetization curve obtained by the CIM was closer to the theoretical curve of M in the thermodynamic limit (solid line) and the theoretical curve of $\sqrt{M^2}$ for the case of $N = 100$ calculated using the DOS obtained by the WL method (dashed line), than the mean-field one (dotted line).

Finally, we performed a numerical simulation using an algorithm based on MF dynamics (noisy MF annealing) [15], whose results are shown by + plots in Fig. 3. Here, we set the standard deviation of the Gaussian noise σ and the amplitude splitting parameter α to the same values in [15] (both 0.15). As expected, the results are close to the MF solution. These observations indicate that the CIM in its present operational condition well simulates the thermodynamic properties of the Ising model, which is presumably hard to reproduce with the MF approach.

It is not yet clear what caused the discrepancy between the estimated temperatures and the thermodynamic temperatures at $\beta > \sim 0.6$ in Fig. 2 (c). A possible reason is the freeze-out effect discussed in [12]. Another possibility is “mode selection”, which was observed in our numerical simulation of the CIM [18]. In this phenomenon, some instances of the Ising model show a tendency that certain spin configurations are more likely to appear when the pump amplitude is relatively large. Such “selected modes” may have prevented the thermodynamic temperature from decreasing below ~ 0.6 . Also, the mode-selection phenomenon may have caused a deviation from the canonical distribution in the low-temperature region, in which in turn may have caused the deviation in the experimental specific heat $C = \beta^2(\langle E^2 \rangle - \langle E \rangle^2)$ from theory in Fig. 2 (d).

In summary, we simulated the phase transition of a 2D square-lattice Ising model on the CIM. We confirmed that for relatively small β , the CIM provides a consistent description of thermal equilibrium Ising spins from multiple viewpoints, namely thermodynamics, statistical mechanics, and statistical inference. With the obtained thermodynamic quantities, we observed a phase-transition-like behavior in a finite-sized system with a transition temperature close to the theoretical value. These results indicate that the CIM is an optical realization of a thermodynamic spin system where all the spins can be independently accessed. We may utilize these characteristics for information processing tasks such as Boltzmann sampling and fast simulation of magnetic systems.

[1] N. Mohseni et al., Nat. Rev. Phys. 4, 363 (2022).

[2] A. Marandi et al., Nat. Photon. 8, 937 (2014).

- [3] T. Inagaki et al., *Science* **354**, 603 (2016).
- [4] P. L. McMahon et al., *Science* **354**, 614 (2016).
- [5] R. Hamerly et al., *Sci. Adv.* **5**, eaau0823 (2019).
- [6] T. Honjo et al., *Sci. Adv.* **7**, eabh0952 (2021).
- [7] D. Pierangeli et al., *Phys. Rev. Lett.* **122**, 213902 (2019).
- [8] F. Böhm et al., *Nat. Commun.* **10**, 3538 (2019).
- [9] M. Babaeian et al., *Nat. Commun.* **10**, 3516 (2019).
- [10] Y. Okawachi et al., *Nat. Commun.* **11**, 4119 (2020).
- [11] T. Inagaki et al., *Nat. Commun.* **12**, 2325 (2021).
- [12] F. Böhm et al., *Nat. Commun.* **9**, 5020 (2018).
- [13] H. Takesue et al., *Phys. Rev. Appl.* **13**, 054059 (2020).
- [14] L. Onsager, *Phys. Rev.* **65**, 117 (1944).
- [15] A. D. King et al., arXiv:1806.08422 (2018).
- [16] F. Wang and D. P. Landau, *Phys. Rev. Lett.* **86**, 2050 (2001).
- [17] E. W. Montroll et al., *J. Math. Phys.* **4**, 308 (1963).
- [18] Y. Yamada and K. Inaba, Adiabatic Quantum Computing Conference (AQC) 2021.